ARTICLE NO. 80-4068

G80-055

Optimal Thrust Control with Proportional Navigation Guidance

0005
0006
0008

Anthony J. Calise*
Drexel University, Philadelphia, Pa.

This paper derives a nonlinear optimal thrust control law for a missile using proportional navigation guidance to intercept a maneuvering target. It is shown that using singular perturbation techniques combined with a multiple time scaling approach leads to a control solution that has an algebraic feedback form. Numerical results are given for a short-range air-launched missile, and comparisons are made to proportional navigation guidance with boost-coast propulsion. The results show that thrust magnitude control (TMC) improves turning performance for missile launches at high aspect angles relative to the target velocity vector and when launching from a lag condition relative to the line-of-sight.

Introduction

In general, missiles may be maneuver limited for launches from high aspect angles off the target tail and/or for launches at a lag condition. The maneuver limit results from a combination of constraints on aerodynamic lift due to limits on control surface deflection, control actuator torque, structural load (G_{max}) and stall angle-of-attack (α_{max}). These limits give rise to large miss distances. They also cause failures in the seeker tracking loop due to high line-of-sight (LOS) rate and large gimbal angles that result from the inability of the missile to establish a collision (or lead) course early in the trajectory.

Dogfight conditions can lead to launches at high aspect angles against highly maneuverable targets. These conditions require highly maneuverable missiles that are light in weight and have adequate range capability. Conventional aerodynamic solutions for increasing lift involve increasing control surface and wing area. However, this tends to increase airframe weight and drag, thereby decreasing missile range capability if total weight is held fixed. Thrust vector control (TVC) can be used to augment lift and provide stable flight at high angles-of-attack without large aerodynamic control surfaces. However, TVC is inefficient from an energy point of view, and the gimballed nozzle and complex autopilot design requirements inexorably lead to increased weight and cost.

The objective of this study is to investigate the performance improvement that can result from the use of thrust magnitude control (TMC) on a conventional missile that utilizes proportional navigation (PN) guidance. In order to establish best performance, an optimal TMC solution is desired. An efficient optimization technique is required since many trajectory solutions are needed to establish missile envelope performance at various altitudes and for various target velocities and maneuvers. A separate but equally important issue is the on-board implementation of the optimal control solution. This requires an essentially analytic solution that permits a feedback implementation.

References 1-5 have considered the optimal TMC problem. In general, analytically tractable solutions were obtained only for horizontal, rectilinear motion[1] and for the case of constant angle-of-attack.[5] Moreover, the authors of Ref. 4 cite the difficulty of obtaining convergence for free time problems using gradient methods of solution. Reference 6 explores the application of singular perturbation methods to optimal TMC and optimal lift control. Nonlinear feedback control solutions are obtained for lift and thrust during a turn to a specified downrange position. This paper extends the analysis in Ref. 6 to the case of a moving terminal point with lift defined by a PN guidance law. The resulting solution is used to define the thrust control in a missile simulation and to generate envelope performance results for a short-range air-to-air missile. Comparisons are made to the same missile with boost-coast propulsion.

Problem Formulation

The equations of motion in the horizontal plane are written in a relative coordinate frame attached to the target velocity vector. The geometry is defined in Fig. 1. The missile state equations are

$$\dot{x} = V\cos\Phi \tag{1}$$

$$\dot{y} = V\sin\Phi - V_T \tag{2}$$

$$\dot{\Phi} = L_n/mV = N\dot{\theta} \tag{3}$$

$$\dot{V} = (T-D)/m \tag{4}$$

where x is cross range position, y is downrange position, Φ is missile heading, V is missile velocity, V_T is target velocity, m is missile mass, T is thrust, D is drag, and L_n is the component of the missile lift vector in the horizontal plane. These equations apply over a flat earth with m constant and thrust directed along the flight path. Drag is a nonlinear function of V and L_n and can be characterized by the classical drag polar form

$$D = qsC_{D_0} + KL^2/qs \tag{5}$$

where C_{D_0} is the zero lift drag coefficient, K is the induced drag coefficient, s is the reference area, L is the total lift expressed as

$$L^2 = W^2 + L_n^2 \tag{6}$$

W is the weight, q is the dynamic pressure

$$q = \tfrac{1}{2}\rho V^2 \tag{7}$$

and ρ is the air density at the launch altitude. Note that the controls in Eqs. (1-4) are L and T.

Received Feb. 8, 1979; revision received Sept. 17, 1979.

Index categories: LV/M Dynamics and Control; LV/M Guidance; Missile Systems.
*Associate Professor, Mechanical Engineering and Mechanics. Member AIAA.

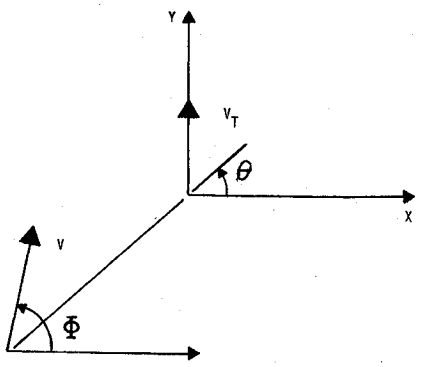

Fig. 1 Two-dimensional geometry for the missile intercept problem formulation.

Present day missiles utilize various forms of PN guidance to effect an intercept. The form taken here is that the missile turn rate $\dot{\Phi}$ is proportional to the LOS rate $\dot{\theta}$ where

$$\dot{\theta} = [V_T \cos\theta - V \sin(\Phi - \theta)]/R \tag{8}$$

$$R = (x^2 + y^2)^{1/2} \tag{9}$$

and N is the navigation gain. In general, PN guidance results in zero miss distance for an infinitely maneuverable missile. With time varying gains, it is optimal in a linear-quadratic (LQ) sense against nonmaneuvering constant velocity targets.[7] Nominal values for N range between 3 and 4. Equations (3), (6), (8), and (9) are used to eliminate L as a control variable, thus only T is optimized. In general, it is desirable to regulate missile velocity so that maneuvers are performed with minimum loss in energy. This can be approximated by minimizing the drag loss.

$$J = \int D\,dt \tag{10}$$

A suitable set of control constraints is

$$|L| \le qsC_{L_{\max}} = qsC_{L_\alpha}\alpha_{\max} \tag{11}$$

$$|L| \le WG_{\max} \tag{12}$$

$$0 \le T \le T_{\max} \tag{13}$$

$$V \ge V_{\min} \tag{14}$$

$C_{L_{\max}}$ is the maximum lift coefficient and is used to represent a stall angle-of-attack limit or a limit due to maximum control surface deflection. $G_{\max}$ represents a load factor limit which may arise due to a structural limit or a control surface actuator limit. $V_{\min}$ is used to insure aerodynamic stability. Due to the PN guidance law, the constraints in Eqs. (11) and (12) translate into constraints on velocity.

In the model described here m and V_T are treated as constants, and the target turn rate is assumed to be zero. Since it is impossible to predict furture target maneuvers, and since PN guidance is only sensitive to the current V_T, it is consistent to treat V_T as a constant and to ignore target turn rate. However, the analytical form of the control solution permits repetitive solution of the optimal problem. Hence, in simulating the true missile and target dynamics, the parameters m and V_T are updated and used as new initial conditions at each integration step. Thus, the resulting control solution is desensitized to variations in unmodeled states and is made reactive to unpredictable target evasive maneuvers.

The boundary conditions on x, y, Φ, and V are the current state values at the initial time, and at the terminal time we enforce

$$x(t_f) = y(t_f) = 0 \tag{15}$$

to ensure intercept.

Singular Perturbation Solution

Following the procedure in Ref. 6, the dynamics in Eqs. (1-4) are scaled as follows:

$$\dot{x} = V\cos\Phi \qquad x(0) = x^0 \tag{16}$$

$$\dot{y} = V\sin\Phi - V_T \qquad y(0) = y^0 \tag{17}$$

$$\epsilon\dot{\Phi} = L_n/mV = N\dot{\theta} \qquad \Phi(0) = \Phi^0 \tag{18}$$

$$\epsilon^2\dot{V} = (T-D)/m \qquad V(0) = V^0 \tag{19}$$

The asymptotic expansion parameter ϵ is nominally equal to 1.0. It is introduced as a time scaling parameter so that the state dynamics are ordered on separate time scales in accordance with the relative speeds with which these variables can change their magnitudes. Here, we imply that x and y dynamics are slow compared to Φ, and the V dynamics are fastest. Higher-order dynamics (control lags, body rates) can be introduced and scaled with higher powers of ϵ. The appendix provides a justification for this ordering by writing the equations of motion in nondimensional form and identifying ϵ with the missile minimum turn radius and maximum thrust-to-weight ratio.

References 6 and 8 show that this procedure reduces to solving a series of first-order optimal control problems for which a feedback (point-wise optimization) solution results. The optimal control and trajectory solution is expanded in an "outer expansion" solution about $\epsilon = 0$:

$$\bullet(t,\epsilon) = \bullet(t,0) + \frac{\partial \bullet}{\partial \epsilon}\epsilon + \cdots\cdots \tag{20}$$

where the $\bullet$ denotes the state, adjoint, and control variables. However, the expansion in Eq. (20) is not uniformly valid in the interval $0 \le t \le t_f$ since the fast states and their adjoints will not satisfy their respective boundary conditions at $t = 0$ and $t = t_f$. This leads to the occurrence of boundary layer or "inner expansion" solutions of the form

$$\bullet(\tau_i,\epsilon) = \bullet(\tau_i,0) + \frac{\partial \bullet}{\partial \epsilon}\epsilon + \cdots\cdot \tag{21}$$

$$\bullet(\sigma_i,\epsilon) = \bullet(\sigma_i,0) + \frac{\partial \bullet}{\partial \epsilon}\epsilon + \cdots\cdot \tag{22}$$

The inner expansion solutions are derived using the time stretching transformations

$$\tau_i = t/\epsilon^i \qquad \sigma_i = (t_f - t)/\epsilon^i \tag{23}$$

about $t = 0$ and $t = t_f$, respectively. The total solution, which in effect is the sum of Eqs. (20-22), satisfies all the boundary conditions and is uniformly valid in the closed interval $0 \le t \le t_f$. It will be seen that boundary layers near $t = t_f$ are not needed for the problem formulation in the previous section.

As a consequence of the parameter ϵ in Eqs. (16-19), the Euler-Lagrange equations become

$$\dot{\lambda}_x = -\partial H/\partial x = 0 \tag{24}$$

$$\dot{\lambda}_y = -\partial H/\partial y = 0 \tag{25}$$

$$\epsilon\dot{\lambda}_\Phi = -\partial H/\partial\Phi \tag{26}$$

$$\epsilon^2\dot{\lambda}_v = -\partial H/\partial V \tag{27}$$

where

$$H=\lambda_x V\cos\Phi+\lambda_y V\sin\Phi+\lambda_\Phi N\dot{\theta}+\lambda_v(T-D)/m$$
$$+D+\text{constraints}=0 \tag{28}$$

In the following analysis, we will temporarily ignore the constraint terms in Eq. (28) and discuss their effect at the end.

Zero-Order Outer Solution

The zero-order necessary conditions for the outer solution are obtained by letting $\epsilon\to 0$ in Eqs. (18), (19), (26), and (27)

$$L_{n_0}=0 \qquad \dot{\theta}_0=0 \tag{29}$$

$$T_0=D_0 \tag{30}$$

$$D_0=qsC_{D_0}+KW^2/qs \tag{31}$$

$$\partial H_0/\partial\Phi=-\lambda_x V\sin\Phi+\lambda_y V\cos\Phi=0 \tag{32}$$

$$\partial H_0/\partial V=\lambda_x\cos\Phi+\lambda_y\sin\Phi+\rho VsC_{D_0}$$
$$-2KW/qVs=0 \tag{33}$$

where

$$H_0=\lambda_x V\cos\Phi+\lambda_y(V\sin\Phi-V_T)+D_0=0 \tag{34}$$

From Eqs. (24) and (25), λ_x and λ_y are constant. This implies that the optimal heading from Eq. (32) is constant. Since the outer solution must satisfy the terminal constraints in Eq. (15), Φ must be chosen as the collision course for whatever optimal velocity is obtained from Eq. (33). From the second condition in Eq. (29) and from Eq. (8) we also have that

$$\sin(\Phi_0-\theta)=V_T\cos\theta/V \qquad \theta=\tan^{-1}(-y^0/-x^0) \tag{35}$$

Using Eqs. (32) and (33) to eliminate λ_x and λ_y in Eq. (34), we have the following nonlinear expression for the optimal intercept velocity

$$\frac{V}{V_T\sin\Phi_0-V}D_0+2\left(qsC_{D_0}-\frac{KW^2}{qs}\right)=0 \tag{36}$$

Note that the optimal V is dependent only on missile parameters and the air density.

Numerical studies of the solution to Eq. (36) for realistic missile parameters have shown that a close approximation is obtained by ignoring induced drag effects ($K=0$). This simplification results in

$$V_0=2V_T\Phi_0 \tag{37}$$

Combining Eqs. (37) and (35), we obtain the following simple expressions for the optimal heading and velocity:

$$\Phi_0=(\theta+90)/2 \tag{38}$$

$$V_0=V_T\sqrt{2(1+\sin\theta)} \tag{39}$$

For a tail attack ($\theta=90$ deg), $\Phi_0=90$ deg and $V_0=2V_T$. For a beam attack ($\theta=0$ or 180 deg), $\Phi=45$ or 145 deg and $V_0=\sqrt{2}V_T$.

The solutions in Eqs. (38) and (39) are inaccurate for a small range of θ about $\theta=-90$ deg, which corresponds to a launch position directly forward of V_T. Note that $V_0=0$ for $\theta=-90$ deg, for which D_0 is infinite were it not for the fact that K was set to zero. In any event, this range of low velocities is eliminated by the constraints in Eqs. (11) and (14), or by the use of the more exact solution for $K\neq 0$.

For the velocity solution to Eq. (36), the adjoints can be obtained from Eqs. (32) and (33) as

$$\lambda_{x_0}=-\cos\Phi_0[\rho V_0 sC_{D_0}-2KW^2/q_0V_0s] \tag{40}$$

$$\lambda_{y_0}=\lambda_{x_0}\tan\Phi_0 \tag{41}$$

The outer solution corresponds to a singular arc of the original control problem. The terminal constraints on x and y are satisfied, and it can be shown that both λ_Φ and λ_v are zero, as is required at the terminal time since both $\Phi(t_f)$ and $V(t_f)$ are free. Hence, to zero-order no boundary layers are required around $t=t_f$ to satisfy the necessary conditions for the original problem.

Zero-Order First Boundary-Layer Solution

For the ϵ scaling in Eqs. (18) and (19), two boundary-layer solutions are required around the initial time. In the first boundary layer, Φ dynamics are modeled and V retains its role as a control variable. To simplify the analysis, the W^2 component in Eq. (6) is ignored. This is also done to be consistent with the approximation made in the outer solution. The necessary conditions are obtained by introducing the time transformation $\tau_1='/\epsilon$ in Eqs. (16-19) and Eqs. (24-27), and letting $\epsilon\to 0$. This results in the following equations:

$$x_1=x_0(0)=x^0 \qquad y_1=y_0(0)=y^0 \tag{42}$$

$$\mathrm{d}/\mathrm{d}\tau_1,\Phi=L_n/mV=N\dot{\theta} \qquad \Phi(0)=\Phi^0 \tag{43}$$

$$T=D \tag{44}$$

$$\lambda_{x_1}=\lambda_{x_0} \qquad \lambda_{y_1}=\lambda_{y_0} \tag{45}$$

$$\mathrm{d}/\mathrm{d}\tau_1,\lambda_\Phi=-\partial H_1/\partial\Phi \tag{46}$$

$$\partial H_1/\partial V=\lambda_{x_0}\cos\Phi+\lambda_{y_0}\sin\Phi-\lambda_\Phi N\sin(\Phi-\theta)/R$$
$$+\rho sC_{D_0}V-4KN^2m^2\dot{\theta}\sin(\Phi-\theta)/\rho sR=0 \tag{47}$$

where

$$H_1=\lambda_{x_0}V\cos\Phi+\lambda_{y_0}(V\sin\Phi-V_T)+\lambda_\Phi N\dot{\theta}+D=0 \tag{48}$$

The optimality conditions in Eqs. (47) and (48) represent two nonlinear equations for the control V_1 and for the adjoint λ_{Φ_1}. The nonlinear equation for V_1 is quadratic in form and has two roots

$$V_1=(-B_1\pm\sqrt{B_1^2-4A_1C_1})/2A_1 \tag{49}$$

where

$$A_1=-\rho s\sin(\Phi-\theta)[C_{D_0}/2+2KD\sin^2(\Phi-\theta)]/V_T \tag{50}$$

$$B_1=\rho s[C_{D_0}+4KD\sin^2(\Phi-\theta)]\cos\theta \tag{51}$$

$$C_1=E\sin(\Phi-\theta)\cos^2\theta+F\cos\theta-\lambda_{y_0}\sin(\Phi-\theta) \tag{52}$$

$$D=N^2m^2/\rho sR^2 \qquad E=-2KV_TD$$

$$F=\lambda_{x_0}\cos\Phi+\lambda_{y_0}\sin\Phi \tag{53}$$

It can be shown that the radical in Eq. (49) approaches zero as $\Phi\to\Phi_0$ and that $V_1\to V_0$. Hence, the boundary layer is asymptotic to the outer solution. Also, both roots of Eq. (49)

are minimizing since from Eq. (47)

$$\partial^2 H_1/\partial V^2 = \rho s C_{D_0} + 4KN^2 m^2 \sin^2(\Phi-\theta)/\rho s R \qquad (54)$$

is independent of V_1; however, it is necessary to always select the positive root. When $|\Phi-\Phi^0|$ is small, it is possible to have two positive roots since both roots are asymptotic to V_0 as $|\Phi-\Phi^0|\to 0$. So, it was decided to always select the positive root closest to V_0. This avoids the occurrence of discontinuities in V_1 and in λ_{ϕ_1}, which are possible only for the case of impulsive thrust.

Zero-Order Second Boundary-Layer Solution

Velocity dynamics are modeled in the second boundary layer, and only the original control variable is optimized. The transformation $\tau_2 = t/\epsilon^2$ is used to obtain the zero-order necessary conditions. Taking the limit as $\epsilon \to 0$ we have

$$x_2 = x^0 \qquad y_2 = y^0 \qquad \Phi_2 = \Phi^0 \qquad (55)$$

$$\mathrm{d}/\mathrm{d}\tau_2 V = (T-D)/m \qquad V(0) = V^0 \qquad (56)$$

$$\lambda_{x_2} = \lambda_{x_0} \qquad \lambda_{y_2} = \lambda_{y_0} \qquad \lambda_{\Phi_2} = \lambda_{\Phi_1}(0) \qquad (57)$$

$$\mathrm{d}/\mathrm{d}\tau_2 \lambda_v = -\partial H_2/\partial V \qquad (58)$$

$$T = \begin{cases} T_{\max} & (\lambda_v < 0) \\ T_{\min} & (\lambda_v > 0) \\ D & (\lambda_v = 0) \end{cases} \qquad (59)$$

where

$$H_2 = \lambda_{x_2} V\cos\Phi + \lambda_{y_2}(V\sin\Phi - V_T) + \lambda_{\Phi_2} N\dot{\theta} + \lambda_v (t-D)/m + D = 0 \qquad (60)$$

From Eq. (59) we see that the outer and first boundary-layer solutions represent the singular arc portion of the optimal control solution. Comparison of Eq. (60) with Eq. (48) shows that $\lambda_v = 0$ and $T = Df$ at $V = V_1(0)$. Since the second boundary-layer solution for V must approach $V_1(0)$, Eq. (59) implies that $\lambda_v < 0$ and $T = T_{\max}$ for $V < V_1(0)$, and $\lambda_v > 0$ and $T = T_{\min}$ for $V > V_1(0)$. The actual value of λ_v can be computed by substitution of V and T in Eq. (60).

For simulation purposes, the singular arc control was approximated by using a proportional control for thrust in the vicinity of $V - V_1 = 0$

$$T = D + K(V_1 - V) \qquad (61)$$

For $|V - V_1| > 100$ ft/s, T was set equal to the appropriate limit.

First-Order Corrections

The necessary conditions in Eqs. (59) and (60) are identical to those of the original control problem with $\epsilon = 1$. Hence, if the states are measured, the solution is exact except that λ_x, λ_y, and λ_Φ are known only to zero-order. As shown in Ref. 6, first-order corrections account for changes in x and y during the heading transition (ignored in the zero-order first boundary layer solution), and for changes in Φ during the velocity transition (ignored in the zero-order second boundary layer solution). The first-order matching conditions can be used to calculate the first-order correction to V_1 and hence, to T. However, since the control solution can be continually updated for the current values of x, y, and Φ, the need for first-order corrections is greatly diminished. In fact, the first-order corrections provided little improvement over the zero-order solution in Ref. 5. The need for a first-order correction is even less here since the lift profile is not optimized.

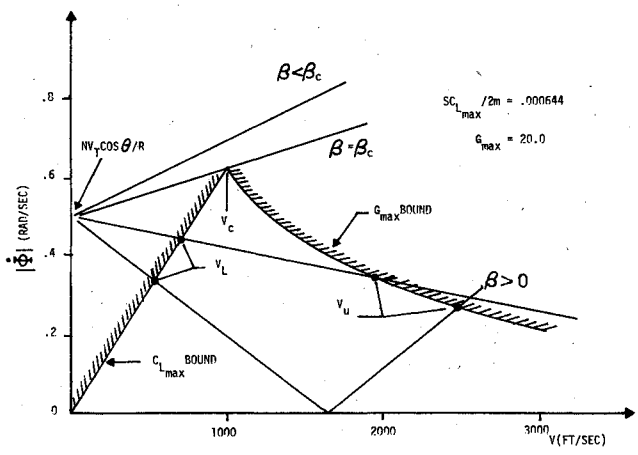

Fig. 2 Relationship between $C_{L_{\max}}$, $G_{\max}$, and the velocity limits for PN guidance.

Enforcing Constraints

The constraints in Eqs. (13) and (14) are enforced when computing V_0 and V_1 in the outer solution and first boundary solutions, and in computing T in the second boundary layer. Constraints (11) and (12) are first transformed to velocity constraints and then enforced along with Eq. (14) in computing V_0 and V_1.

Figure 2 shows the relationship between $G_{\max}$, $C_{L_{\max}}$, and the corresponding lower (V_L) and upper (V_U) velocity limits. From Eqs. (3) and (8), we have that the absolute magnitude of the missile heading rate is a linear function of missile velocity

$$|\dot{\Phi}| = N|V_T\cos\theta - V\sin\beta|/R \qquad \beta = \Phi - \theta \qquad (62)$$

Equation (3) can also be used to relate $|\dot{\Phi}|$ to $C_{L_{\max}}$ and $G_{\max}$

$$|\dot{\Phi}| \le (\rho s C_{L_{\max}}/2m)V \qquad (63)$$

$$|\dot{\Phi}| \le g G_{\max}/V \qquad (64)$$

The intersection of Eq. (62) with Eqs. (63) and (64) provides V_L and V_U† The intersection of Eqs. (63) and (64) provides the maximum attainable $|\dot{\Phi}|$ and the corresponding corner velocity (V_c). From Eq. (62) and Fig. 2 it is apparent that the velocity control is critically important at high aspect-angles (θ near 0 or 180 deg), short ranges, and at lag angles ($\beta < 0$). As shown in Fig. 2, there is a critical lag angle β_c beyond which the missile cannot maintain the prescribed PN guidance law. For $\beta < \beta_c$, $V_1 = V_c$ is adopted for the control solution in the first boundary layer.

To summarize, the approach to enforcing the velocity constraints is as follows:

1) Calculate the unconstrained solutions for V_0 and V_1.

2) Calculate V_L and V_U, and use these along with $V_{\min}$ to limit V_0 and V_1.

3) On the constraint bound, calculate λ_{x0}, λ_{y0}, λ_{Φ_0} by substitution of the constrained values for V_0 and V_1 into Eqs. (34) and (48).

Numerical Results

This section presents two examples illustrating the potential performance improvements that can result from the implementation of TMC on air-launched tactical missiles. The first example shows the effect the TMC has on increasing the

†Note from Fig. 2 that there can be three intersections of Eqs. (62) and (64). The first intersection is used to establish V_U since the missile will not have sufficient propulsion to attain the higher velocity solutions.

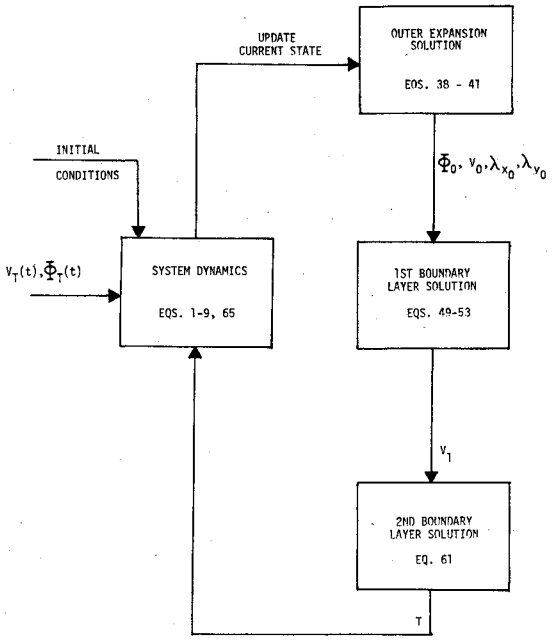

Fig. 3 Feedback implementation of the singular perturbation solution.

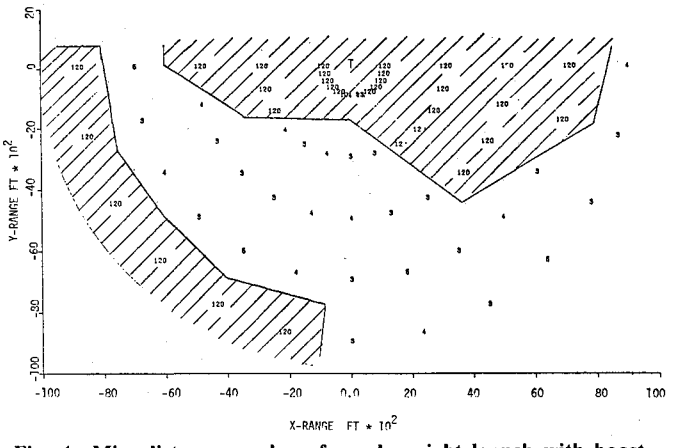

Fig. 4 Miss distance envelope for a boresight launch with boost-coast propulsion.

missile launch envelope. The second example shows that TMC is effective in reducing the track crossing angle (TCA) at intercept.‡

Optimal Thrust Control Simulation

The previous section derived the nonlinear expressions for the optimal thrust control to zero order. These can be used in a feedback form by treating the current state values as new initial conditions. Figure 3 diagrams a computer implementation of the thrust control equations with a simulation of the original system dynamics [see Eqs. (1-9)] plus an additional equation to model mass variations

$$\dot{m} = -cT \tag{65}$$

The control computations are updated at each integration step. The missile aerodynamic and propulsion parameters were chosen as follows: $\rho = 0.0017$ slugs/ft^3 (alt. = 10,000 ft), launch weight = 200 lb, propellant weight = 50 lb, $c = 0.01$,

‡The TCA is the angle between the missile and target velocity vectors at intercept.

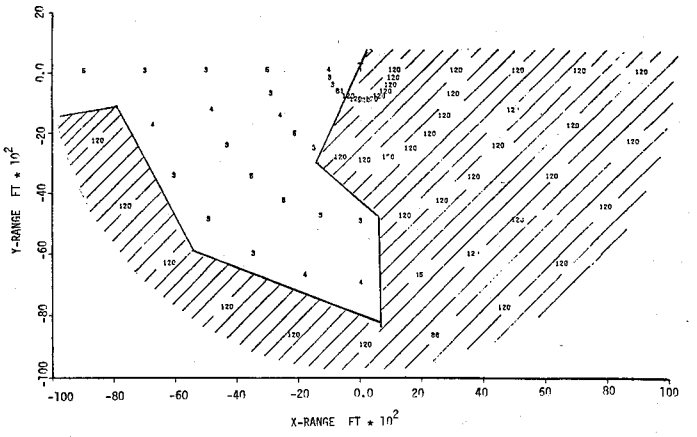

Fig. 5 Miss distance envelope for a 20-deg off-boresight launch with boost-coast propulsion.

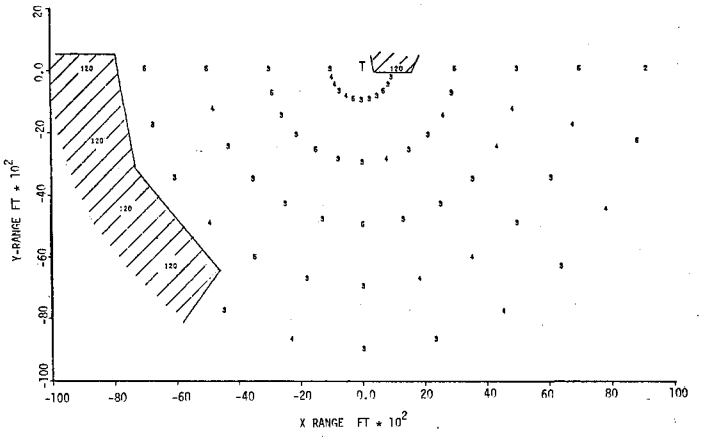

Fig. 6 Miss distance envelope for a boresight launch with optimal TMC.

$C_{D_0} = 1.2$, $K = 0.02$, $s = 0.17$ ft^2, $T_{max} = 5000$ lb, $T_{min} = 0$ lb, $C_{L_{max}} = 25$, $G_{max} = 25$.

These parameters correspond to Missile-II of Ref. 6. The propellant weight is enforced by setting $T = 0$ if and when the missile weight is decreased to 150 lb. The thrust was also constrained to $T = T_{max}$ for the first 0.5 s to insure a safe separation from the launch aircraft. The initial target and missile velocities in all cases was 1000 ft/s.

Example Envelope Results

Figures 4 and 5 depict miss distance data corresponding to different ranges and aspect-angles-off at launch for a missile with PN guidance and with boost-coast propulsion. Miss distances greater than 120 ft are shown as 120, and miss distances less than 5 ft result from arbitrary termination of the simulation when the range is less than 5 ft. The regions of miss are shaded. The target is initially located at X-RANGE = Y-RANGE = 0.0 and is executing a 7.0 g maneuver to the right. Figure 4 corresponds to launching with the missile velocity vector along the initial LOS, and Fig. 5 has the initial missile velocity vector rotated 20 deg counterclockwise from the initial LOS. Note that a launch from anywhere in the right-hand quadrant in Fig. 5 results in a miss. This is due to the severe maneuver requirement placed on the missile when launching from a lag condition. The missile is on the g limit and cannot maintain PN. The region on the left of Fig. 5 is not significant since an intelligent target would maneuver to the left for this set of launch conditions.

With optimal TMC, the missile can be controlled to fly near the corner velocity (V_c) when executing the initial turn and accelerated when the LOS rate is sufficiently reduced. This

Table 1 Comparison of track crossing angle (deg) for boost-coast propulsion and optimal thrust magnitude control

Aspect angle at launch, deg	Boost-coast			Optimal TMC		
	$N=4$	$N=2$	$N=1$	$N=4$	$N=2$	$N=1$
0	19.3	14.4	*M*	21.2	16.3	0
30	32.8	23.4	*M*	35.9	25.7	0.2
60	46.7	35.6	*M*	50.5	37.7	0.1
90	*M*	*M*	*M*	61.7	54.5	*M*

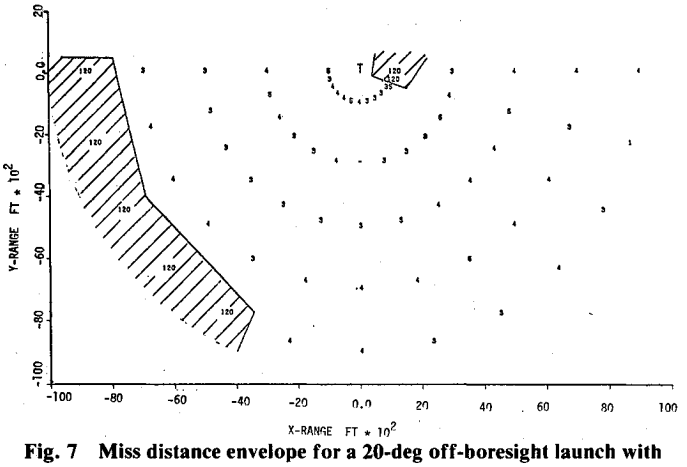

Fig. 7 Miss distance envelope for a 20-deg off-boresight launch with optimal TMC.

allows the missile to maintain PN by increasing the turn rate limit and simultaneously decreasing the LOS rate when flying at a lag condition. Figures 6 and 7 give the miss distance results for the same missile launched from the same conditions as in Figs. 4 and 5. Note that the maneuver limited region of miss is almost completely eliminated, and that the miss at long ranges due to propulsion limits is not significantly altered.

Example TCA Results

Reduction of TCA's at intercept greatly relaxes sensor and warhead fusing requirements, and ultimately leads to improved missile lethality. With PN guidance, the TCA increases with lag angle, aspect-angle-off,§ and range at launch. The TCA can be reduced by reducing the navigation gain N. However, this leads to high missile turn rates just prior to intercept. Reducing N to 1.0 results in a pure-pursuit ($\beta=0$) type of trajectory for boresight launches, and a zero TCA for an infinitely maneuverable missile.

Simply reducing N is not recommended as the best approach to reducing TCA's however, it is interesting to see what effect TMC has on the outcome. The effect of reducing N for both boost-coast propulsion and optimal TMC is shown in Table 1. These results were generated for boresight launch at a fixed launch range of 5000 ft and for varying values of aspect angle. The target performs a 5 g maneuver into the attack. Note that most of the reduction in TCA's occurs for $1.0<N<2.0$. Using boost-coast propulsion results in a miss (M) due to g saturation. Optimal TMC allows higher turn rates and lower TCA's by gradually reducing V towards V_c prior to intercept.

Summary

This paper uses singular perturbation concepts combined with a multiple time scaling analysis procedure to evaluate the importance of thrust magnitude control (TMC) in short-range air-to-air missiles. To perform this evaluation, a nonlinear optimal TMC solution is derived and used as a feedback missile thrust control law in a two-dimensional, point mass simulation of missile and target aircraft dynamics. TMC is compared to conventional boost-coast propulsion. Conventional proportional navigation guidance is assumed in both cases. Significant improvements in missile launch envelope are found for high aspect-angle, short range launches, and for launches from a lag condition. The principal advantage of TMC is that it provides increased maneuverability through control of missile velocity. Range capability is not significantly increased.

The analysis in this paper extends the results in Ref. 6 to the case of a maneuvering terminal point and a proportional navigation aerodynamic control law. Further possible extensions of this analysis include the following: 1) aerodynamic parameter dependence on velocity and altitude; 2) mass dynamics dependence on thrust; 3) optimization of the guidance law.

The analysis described here has been extended to the case of three-dimensional dynamics, and a study of the effects of seeker tracking limits is reported in Ref. 9.

Appendix: Relating the Expansion Parameter to System Parameters

In this appendix, the ordering in Eqs. (16-19) is justified by expressing the state dynamics in nondimensional form and identifying ϵ with physical system parameters. To accomplish this the following nondimensional state variables are defined:

$$x_1=x/R_0 \quad y_1=y/R_0 \quad \phi_1=\phi \quad V_1=V/V_c \quad V_T'=V_T/V_C \tag{A1}$$

where R_0 is the initial range and V_c is the "corner velocity," or the velocity corresponding max turn rate, as shown in Fig. 2. V_c is related to the minimum turn radius ($r_{\min}$) and the maximum turn rate by

$$V_c=r_{\min}\dot{\phi}_{\max} \tag{A2}$$

$$\dot{\phi}_{\max}=g\sqrt{G_{\max}^2-1}/V_c \tag{A3}$$

where Eq. (A3) follows from Eqs. (3), (6), and (12). From Eqs. (A2) and (A3) we also have that

$$r_{\min}=V_c^2/g\sqrt{G_{\max}^2-1}\simeq V_c^2/gG_{\max} \tag{A4}$$

for reasonable values of $G_{\max}$. In addition, we define the dimensionless time variable

$$t_1=(V_c/R_0)t \tag{A5}$$

the dimensionless drag parameters

$$C_{D_0}^1=C_{D_0}/C_{L_{\max}} \qquad K_1=KC_{L_{\max}} \tag{A6}$$

§Aspect-angle-off is defined as the angle between the LOS and the target velocity vector.

and the dimensionless controls

$$T_1 = T/T_{\max} = T/W\eta_{\max} \tag{A7}$$

$$L_1 = L/WG_{\max} \tag{A8}$$

where

$$\eta_{\max} = T_{\max}/W \tag{A9}$$

Note that if we similarly define

$$L_{n_1} = L_n/WG_{\max} \tag{A10}$$

then

$$L_{n_1}^2 = (L^2 - W^2)/W^2G_{\max}^2 \simeq L_1^2 \tag{A11}$$

Equations (9-12) in the nondimensional variables become

$$\mathrm{d}/\mathrm{d}t_1 x_1 = V_1 \cos\phi_1 \tag{A12}$$

$$\mathrm{d}/\mathrm{d}t_1 y_1 = V_1 \sin\phi_1 - V_T' \tag{A13}$$

$$\left(\frac{r_{\min}}{R_0}\right)\frac{\mathrm{d}}{\mathrm{d}t_1}\phi_1 = L_1/V_1 \tag{A14}$$

$$\frac{1}{\eta_{\max}}\left(\frac{r_{\min}}{R_0}\right)\frac{\mathrm{d}}{\mathrm{d}t_1}V_1 = \frac{T_1}{G_{\max}} - \frac{D_1}{\eta_{\max}} \tag{A15}$$

We now identify ϵ as

$$\epsilon = r_{\min}/R_0 = k/\eta_{\max} \tag{A16}$$

where k is 0(1). In taking lim $\epsilon \to 0$, we adopt the point of view that both R_0 and $\eta_{\max} \to \infty$. With these definitions, Eqs. (A14) and (A15) can be written as

$$\epsilon\,\mathrm{d}/\mathrm{d}t_1 \phi_1 = L_1/V_1 \tag{A17}$$

$$\epsilon^2 \frac{\mathrm{d}}{\mathrm{d}t_1}V_1 = \frac{kT_1}{G_{\max}} - \epsilon D_1 \tag{A18}$$

where

$$D_1 = V_1^2 C_{D_0}^1 + K_1 L_{n_1}^2 \tag{A19}$$

The performance index [see Eq. (19)] in the nondimensional variables becomes

$$J = \int D_1 \,\mathrm{d}t_1 \tag{A20}$$

and the constraints are

$$0 \le T_1 \le 1 \qquad 0 \le L_1 \le 1 \tag{A21}$$

It can easily be verified that a singular perturbation analysis of the preceding formulation leads to the same control solution as that obtained using the artificial scaling approach.

Acknowledgments

This work was performed while the author was with Dynamics Research Corporation, Wilmington, Mass.

References

[1] Salmon, D.M., Meier, L., and McReynolds, S.R., "A Preliminary Evaluation of Thrust Magnitude Control for Bomber Defense Missiles," Final Report AFOSR F44620-71-C-0018, July 1971.

[2] Matuszewski, J.P., and Asher, R.B., "Use of Thrust Magnitude Control for Strategic and Tactical Missiles," ASD/XR 73-8, June 1973.

[3] Vinh, N.X., Powers, W.F., and Shieh, C.J., "Optimal Aerodynamic and Thrust Magnitude Control of Maneuvering Rockets," AFOSR Grant 71-2129, Sept. 1972.

[4] Powers, W.F. and Shieh, C.J., "Improved Convergence of Gradient-Type Methods Involving Free Final Time and Penalty Functions," AIAA Paper 76-153, 14th Aerospace Sciences Meeting, Jan. 26-28, 1976.

[5] Hermesh, R., Katzir, S., and Kreindler, E., "Optimal Thrust for Maximal Rocket Turn," *Journal of Guidance and Control,* Vol. 2, July-Aug. 1979, pp. 301-307.

[6] Calise, A.J., "A Singular Perturbation Analysis of Optimal Aerodynamic and Thrust Magnitude Control," *Proceedings of the Joint Automatic Control Conference,* San Francisco, Calif., June 22-24, 1977, pp. 1248-1260; to appear in *IEEE Transactions on Automatic Control.*

[7] Kreindler, E., "Optimality of Proportional Navigation," *AIAA Journal,* Vol. 11, June 1973, pp. 878-880.

[8] Calise, A.J., "Extended Energy Management for Flight Performance Optimization," *AIAA Journal,* Vol. 15, March 1977, pp. 314-321.

[9] Goldstein, F. and Calise, A.J., "Nonlinear State Feedback Control for Near Optimal Intercept in Three Dimensions," AIAA Paper 79-1673, AIAA Atmospheric Flight Mechanics Conference, Aug. 6-8, 1979, pp. 368-378.